Vol. 25 • No. 5 • February 4 • 2015

www.afm-journal.de

ADVANCED FUNCTIONAL MATERIALS

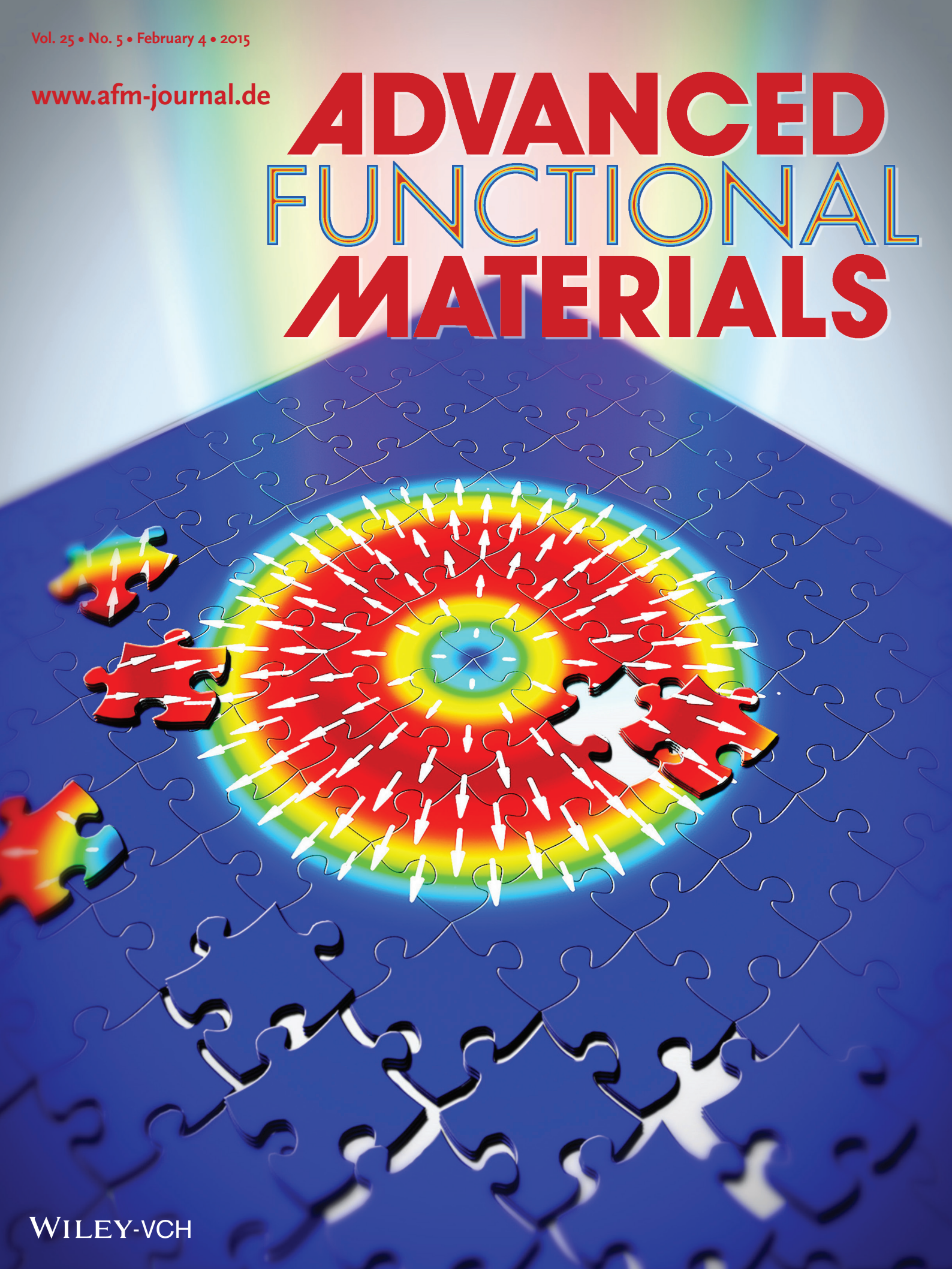

WILEY-VCH

FULL PAPER

Simultaneous Control of Light Polarization and Phase Distributions Using Plasmonic Metasurfaces

Jianxiong Li, Shuqi Chen, Haifang Yang, Junjie Li, Ping Yu, Hua Cheng, Changzhi Gu, Hou-Tong Chen, and Jianguo Tian**

Harnessing light for modern photonic applications often involves the control and manipulation of light polarization and phase. Traditional methods require a combination of multiple discrete optical components, each of which contributes to a specific functionality. Here, plasmonic metasurfaces are proposed that accomplish the simultaneous manipulation of polarization and phase of the transmitted light. Arbitrary spatial field distribution of the optical phase and polarization direction can be obtained. The multifunctional metasurfaces are validated by demonstrating a broadband near-perfect anomalous refraction with controllable linear polarization through introducing a constant phase gradient along the interface. Furthermore, the power of the proposed metasurfaces is demonstrated by generating a radially polarized beam. The new degrees of freedom of metasurfaces facilitate arbitrary manipulation of light and will profoundly affect a wide range of photonic applications.

1. Introduction

Harnessing light for modern photonic applications often involves the control and manipulation of light polarization and phase. The polarization and phase are among the basic properties of light, and their manipulation enables many optical applications and plays an increasingly important role in investigating light-matter interactions.[1–3] Traditional approaches to controlling the light polarization states employ the birefringence and total internal reflection in crystals and polymers, which were used in many wave-plates and Glan–Taylor prisms.[4] Control of light phase, or more generally arbitrary wavefront shaping, relies on the geometrical shape or variation of the spatial profile of the refractive index, such as in lenses, prisms, gratings and holograms. Moreover, the combination of multiple discrete optical devices[5,6] is required to enable simultaneous manipulation of polarization states and phase profile, each of which contributes to a specific function. These components using conventional methods are bulky and very often operate only within a narrow wavelength range, resulting in difficulties in optical system miniaturization and integration, insufficient for emerging technologies with increasingly demanding requirements.

Plasmonic metamaterials have enabled the realization of numerous fascinating phenomena and functionalities simply through tailoring the subwavelength structures and their interactions.[7–9] Taking advantage of the anisotropic response, plasmonic metasurfaces were introduced recently to enable an abrupt phase discontinuity and gradient of the cross-polarized component.[10] Together with the broadband operation and improved linear polarization conversion efficiency,[11] these developments have opened a new research realm of flat optics.[12] However, so far it is still challenging to simultaneously manipulate the polarization state into an arbitrary direction and a phase variation spanning over the entire 2π range. That is, they are still two separate functions requiring different optical devices.[13–21]

Here, we propose and validate dual-layer plasmonic metasurfaces that can provide simultaneous manipulation of the phase and polarization of the transmitted light. An arbitrary spatial field distribution of the optical phase is obtained by using plasmonic metasurfaces consisting of six sub-units, where the orientation of these sub-units can be tuned to further control the polarization. We demonstrate broadband near-perfect anomalous refraction of the transmitted light with high efficiency and to any desired polarization direction. The proposed metasurfaces further facilitate the generation of arbitrary vector optical fields, e.g., a radially polarized beam as demonstrated in our experiments. The new degrees of freedom of metasurfaces facilitate arbitrary manipulation of light and will profoundly affect a wide range of photonic applications.

2. Results and Discussion

Figures 1a,b schematically illustrate the structure of the plasmonic metasurfaces, where the unit cell consists of a pair of

J. Li, Prof. S. Chen, P. Yu, Prof. H. Cheng, Prof. J. Tian
Laboratory of Weak Light Nonlinear Photonics
Ministry of Education
School of Physics and Teda Applied Physics Institute
Nankai University
Tianjin 300071, China
E-mail: schen@nankai.edu.cn; jjtian@nankai.edu.cn
Prof. H. Yang, Prof. J. Li, Prof. C. Gu
Beijing National Laboratory for Condensed Matter Physics
Institute of Physics
Chinese Academy of Sciences
P.O.Box 603, Beijing 100190, China
Dr. H.-T. Chen
Center for Integrated Nanotechnologies
Los Alamos National Laboratory
Los Alamos, NM 87545, USA

DOI: 10.1002/adfm.201403669

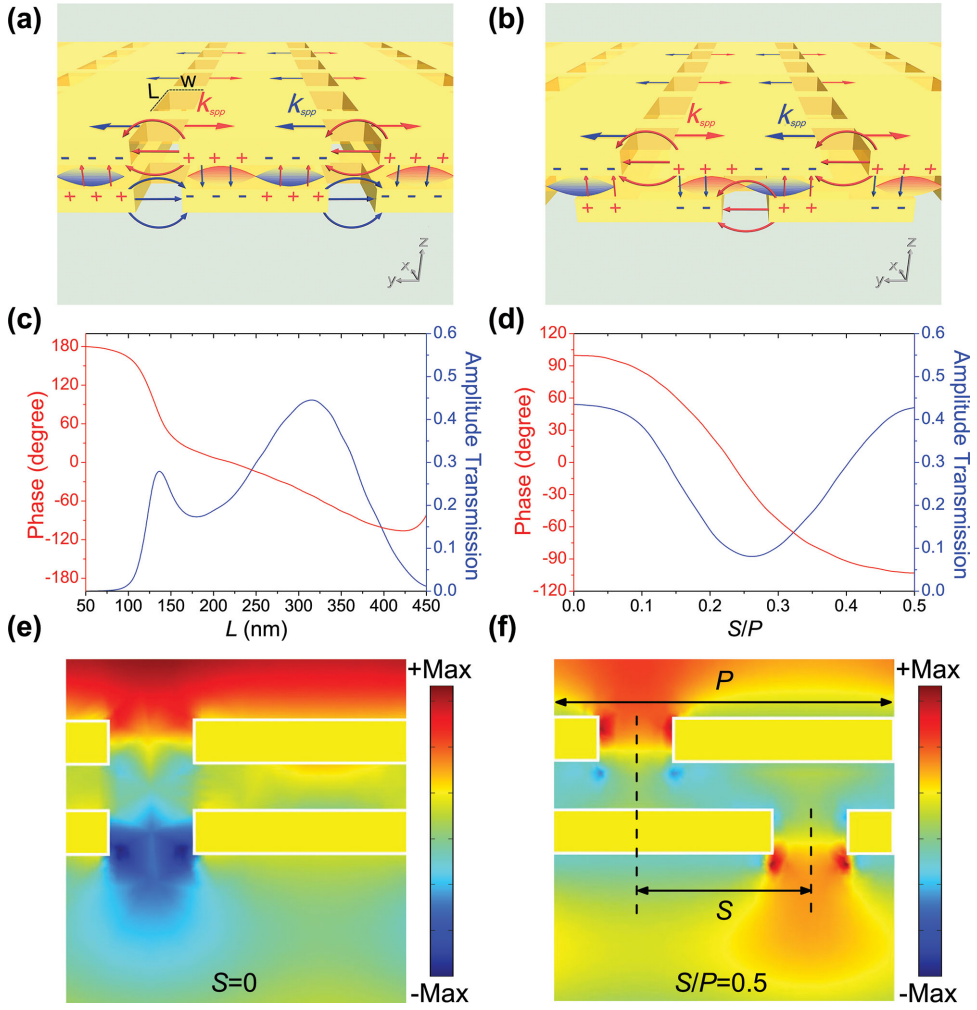

Figure 1. Schematic illustration of the plasmonic metasurfaces a) with aligned nano-aperture pairs and b) with nano-aperture laterally translated. The rectangular nano-apertures in two layers have the same dimensions. The surface plasmonic standing wave is shown between the two metallic structures, with the field and charge oscillation indicated. c,d) Calculated phase (red curves) and amplitude (blue curves) of the transmitted light from the plasmonic metasurfaces as functions of aperture length L for the aligned structure ($S = 0$) with $W = 130$ nm (c) and as functions of lateral translation S for the structure with aperture length $L = 300$ nm and width $W = 130$ nm (d). e,f) Simulated E_y field patterns for the aligned and translated nano-apertures in the y-z plane, with the periods $P_x = 400$ nm and $P_y = 530$ nm, and $L = 300$ nm and $W = 130$ nm.

rectangular nano-apertures in the two 70-nm-thick gold films separated by 70 nm. The top and bottom nano-apertures are either aligned or laterally translated by S in the y-direction, and the whole structure is embedded within silicon dioxide. Surface plasmon polaritons (SPPs) can be excited at each of the metal-dielectric interfaces by the normally incident light polarized in the y-direction. A standing wave of SPPs is formed due to the coupling between the two metal layers resulting in a metal-insulator-metal (MIM) waveguide (see Figure S1, Supporting Information) where the amplitude and phase of the transmitted light are sensitive to the structure geometry and dimensions.[22] For instance, in the aligned case (i.e., $S = 0$) we obtain a large range of phase shifting by tuning the aperture length L, as shown by the finite-element simulations (see Supporting Information) in Figure 1c where relatively high transmission amplitude is maintained over a wide range of L because of the excitation of surface waves and localized resonance.[23]

The range of phase shifting can be further extended by tuning the lateral translation S between the nano-apertures. The simulated transmission amplitude shown in Figure 1d as a function of S exhibits two out-coupling maxima located at $S = 0$ and $S = P/2$ where $P = 530$ nm is the period in the y-direction. This is because the strongest charge oscillation can be established within the bottom individual nano-apertures, resulting in efficient dipole radiation in the transmission direction. Furthermore, the transmissions under these two conditions have a phase difference close to π shown in Figure 1d–f (also see Figure S2), which could be understood through a straightforward analysis of the charge oscillations at the bottom nano-apertures exhibiting opposite directions, as shown by the blue arrows in Figures 1a and b. Therefore, the proposed dual-layer plasmonic metasurfaces offer an effective control of the transmission phase simply through tuning the parameters L and S. Under illumination of normally incident light with linear polarization perpendicular to the major axis of

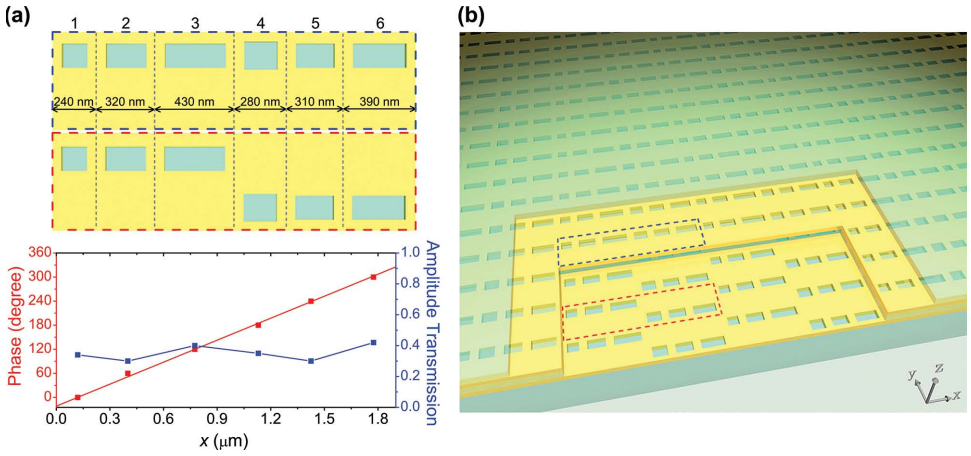

Figure 2. a) Upper panel: Schematics of the top and bottom nano-apertures forming the super-unit-cell in the plasmonic metasurfaces for the demonstration of anomalous refraction. The optimized geometrical parameters of the nano-apertures are L = 140, 220, 330, 180, 210, and 290 nm with corresponding W = 130, 130, 130, 150, 130, and 130 nm. The dimensions of the sub-units in y-direction are 530 nm and in x-direction are specified in the figure. The lateral translation S for the first and second three nano-aperture pairs is 0 and 265 nm, respectively. Lower panel: The transmission phase and amplitude of each nano-aperture pair, calculated under y-polarized incident light at 900 nm. The solid line represents the linear gradient phase. b) Three-dimensional schematic view of the designed plasmonic metasurfaces creating a linear phase gradient profile. Some parts of the silicon dioxide and Au film are uncovered to reveal the details of nano-apertures.

the nano-apertures, the dual-layer plasmonic metasurfaces do not need to convert the polarization to its cross-direction, in marked contrast to many existing proposals employing anisotropic resonators.[10,11] In case of circularly polarized incident light, the field component along the major axis will be simply filtered out (see Figures S3,S4, Supporting Information) based on two facts: (i) different localized resonance within the individual nano-apertures due to their rectangular geometry, and (ii) different surface plasmon resonance due to the different periods in x and y directions. The overall result is that we are able to simultaneously control the polarization and phase of the transmitted light: The orientation of the rectangular nano-apertures determines the polarization through filtering and the geometric parameters (S and L) tune the phase.

In order to validate the ability of nano-aperture pairs in control of phase and polarization, we first use six nano-aperture pairs to form a super-unit-cell as shown by the top panel in **Figure 2**a and create plasmonic metasurfaces schematically illustrated in Figure 2b, realizing near-perfect anomalous refraction. For plasmonic metasurfaces consisting of a periodic array of individual sub-units, they have similar transmission amplitude and a phase increment of $\pi/3$ covering the entire 2π range, as shown by the lower panel in Figure 2a, at the designed operational wavelength of 900 nm. In such a way we create a constant phase gradient along the metasurface to accomplish anomalous refraction (see Figure S5, Supporting Information), for the incident light with circular polarization or linear polarization perpendicular the major axis of the nano-apertures. Due to the filtering effect, we expect the near-complete elimination of transmission in the normal direction, and the anomalous refraction is linearly polarized perpendicular to the nano-aperture major axis. Also note that we have slightly different sub-unit sizes in the x direction for the six nano-aperture pairs in order to form a more compact super-unit-cell, where the phase along the interface can be still approximately considered as a linear phase gradient as shown in the lower panel of Figure 2a. Our simulated and experimental results demonstrate that such an arrangement of the metasurface accomplish anomalous refraction with high efficiency and larger deflection angle, as will be shown below.

Figure 3a shows the scanning electron microscopy (SEM) images of the metasurface structure, which was fabricated by sputtering deposition of gold and silicon dioxide, electron-beam lithography, and reactive ion etching. The fabricated plasmonic metasurface was characterized by performing far-field transmission measurements as a function of the observation angle for normally incident circularly polarized light at 900 nm wavelength (see inset to Figure 3b). The experimental transmission presented in Figure 3b shows only one anomalous refraction peak at 27°, and the ordinary transmission at 0° is completely eliminated. The measured anomalous refraction angle is consistent with our structure design to create a constant phase gradient along the metasurface resulting in an anomalous refraction angle of 27.2°. Our experimental and simulated (see Figure S5) results also show that the polarization of the anomalously refracted light is linear polarized and perpendicular to the major axis of the rectangular nano-apertures, and the dislocation between the nano-aperture layers has minimal effect on the anomalous refraction.

It turns out that the anomalous refraction of the plasmonic metasurface can operate at various incident angles (Figure 3c) and over a wide wavelength range (Figure 3d) (also see Figure S6, Supporting Information), with high transmission efficiency. The measurement results are in good agreement with the theoretical predictions. Measurements and simulations show that the plasmonic metasurface exhibits efficiencies of about 21.4% and 30% for linearly polarized normal incidence at 900 nm, respectively. This discrepancy may be caused dominantly by the inevitable structural imperfections of the fabricated sample shown in Figure 3a, and possibly higher losses in our deposited materials. The near-perfect anomalous refraction realized here directly demonstrates the ability of proposed

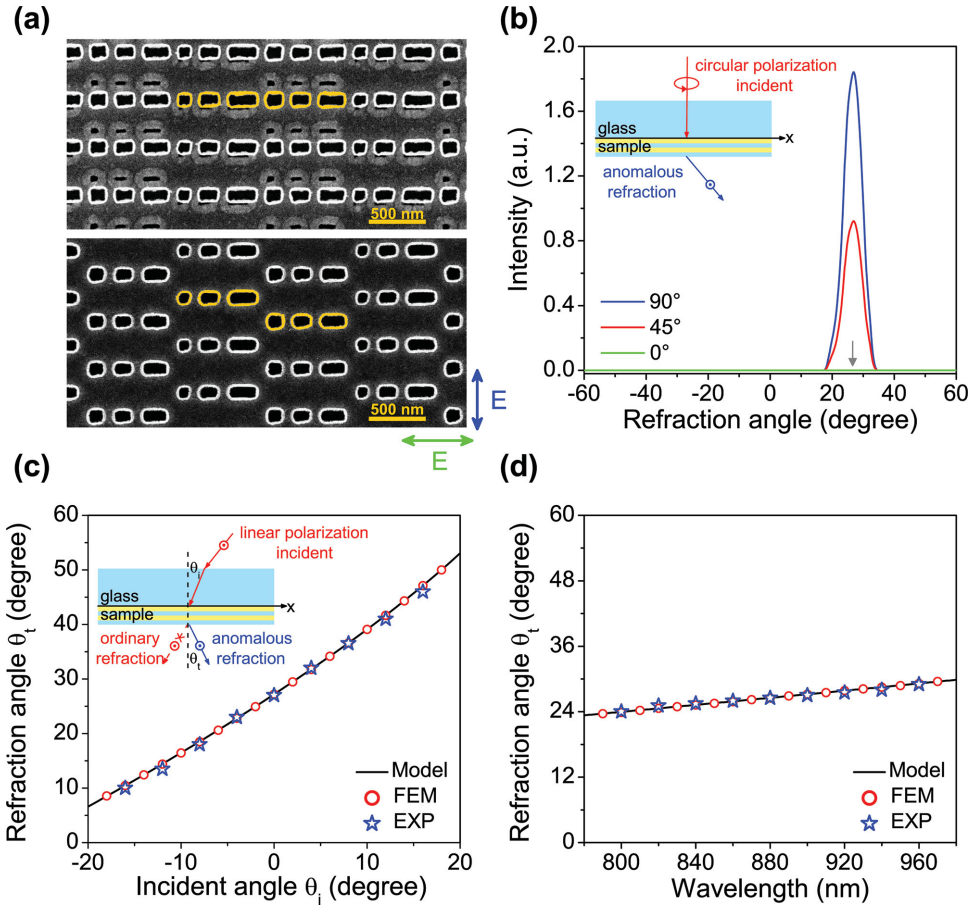

Figure 3. a) SEM images of a fabricated plasmonic metasurface. Top panel: after finishing the whole fabrication; lower panel: after finishing the first layer. The super-unit-cell in each layer is highlighted in yellow. b) Experimentally measured transmission spectra as a function of observation angle for circularly polarized incident light. The three curves are for different angles of the analyzer with respect to major axis of the rectangular apertures. The gray arrow indicates the calculated angle of anomalous refraction based on the generalized Snell's law. c,d) Experimentally (EXP) measured, finite element method (FEM) simulated, and theoretical calculated (Model) anomalous refraction angle as a function of incident angle for 900 nm incident wavelength) (c) and wavelength for normal incidence (d). The insets in (b) and (c) are the schematic illustration of anomalous refraction by plasmonic metasurface.

plasmonic metasurface in controlling the phase of transmitted light, and thereby manipulating the propagation direction, with additional arbitrary control of the linear polarization states, in contrast to many previous metasurfaces that only work for the orthogonal portion of the polarization and lead to simultaneous existence of anomalous and ordinary refractions.[10–21]

The simultaneous control of transmission phase and the polarization direction of the transmitted light provides further opportunity in generating arbitrary vector optical fields. In order to elucidate the underlying operation principle, we consider the thirty-six units shown in **Figure 4**. In the process of polarization filtering from a circularly polarized beam to a linearly polarized beam using the elements in each row, an additional phase term (Pancharatnam–Berry phase), $e^{i\theta}$, is introduced to the transmitted light, where θ is the angle of rotation.[24,25] In addition, the six nano-aperture pairs shown in each column have a conjugate phase increment of $e^{-i\theta}$, which is used to compensate the Pancharatnam–Berry phase. The overall result is that the six nano-aperture pairs in the column have identical phase and similar transmission amplitude, but with varying polarization direction, even though they have different orientation and dimensions. Therefore, the thirty-six nano-aperture pairs enable arbitrary phase tuning spanning the entire 2π range with an increment of $\pi/3$, and polarization direction covering the 360° angle with an increment of 60°.

Many previous metasurfaces can usually be used to generate optical vortex beams.[3,26] Taking advantage of our design of plasmonic metasurfaces for polarization and phase control, we are able to generate arbitrary vector optical fields, e.g., here the radially polarized beam from normally incident circularly polarized light by appropriately arranging the nano-apertures as shown in **Figures 5**a and b. The six regions corresponding to the six different nano-aperture pairs are shown in the most left column of Figure 4. Their orientation angles are configured such that under circularly polarized incident light the transmission is linearly polarized in the radial direction. In addition, the transmission phase difference between these six nano-apertures is completely compensated by the Pancharatnam–Berry phase resulting from the nano-aperture orientation, i.e., the transmissions through the six metasurface regions are all in-phase with

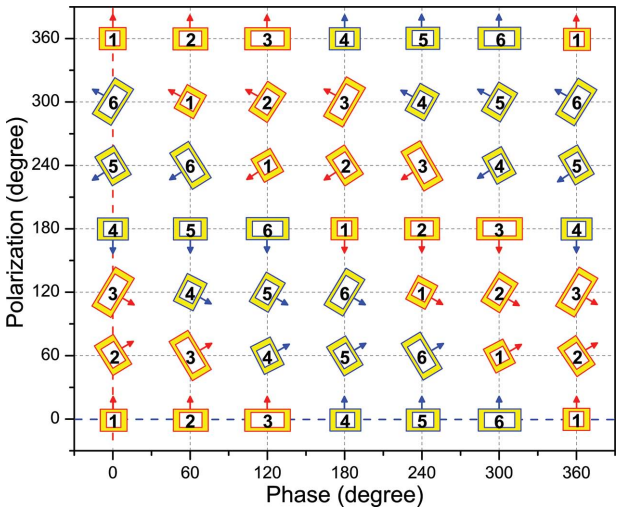

Figure 4. Thirty-six nano-aperture pairs with various dimensions and orientations to construct metasurfaces for the full control of polarization and phase of the transmitted light. The red (blue) frames indicate the aligned (laterally translated) nano-aperture pairs. The transmission phase (without considering the Pancharatnam-Berry phase) is defined to be 0° when the incident electric field is polarized along the arrow directions. The numbers shown in the nano-apertures indicate they have the same dimensions and lateral translation as in the corresponding units in Figure 2a.

radially linear polarization. Viewed by a mid-infrared camera with the experimental schematic shown in Figure 5c, this metasurface profile results in a radially polarized beam, as shown by the doughnut intensity profile in the cross-section (Figure 5d, left panel), a characteristic of the radially polarized beam. The radial polarization is further verified by measuring the beam intensity profiles through adding and rotating a linear analyzer in front of the detector. The measured patterns shown in Figure 5d are consistent with typical radially polarized beams, while their deviation from the perfect beam intensity profiles is due to the facts that we used only six types of nano-aperture pairs, which can be resolved by increasing the number of appropriately designed sub-units to improve the spatial resolution, as well as the imperfection of the fabricated metasurface structure, which will be less severe when working at longer wavelengths such as in the mid-infrared, terahertz and microwave regimes. In virtue of the simultaneous control of phase and polarization spanning the entire 2π range, we can use the designed plasmonic metasurfaces to generate standard radially polarized beam in absence of Pancharatnam–Berry phase, instead of the twisted vector optical field carrying a helical phase.[27] Through simple arrangement of the thirty-six nano-aperture pairs, we can also realize vector optical fields with more complex and non-regularly spatial distribution in phase and polarization, which will not be influenced by the Pancharatnam–Berry phase (see Figure S7 and Movies S1–S3, Supporting Information).

3. Conclusion

In summary, we have proposed and experimentally validated plasmonic metasurfaces achieving simultaneous control of the phase and polarization direction of light. For linearly polarized incident light, the metasurface enables near-perfect anomalous refraction without converting the polarization to its cross-direction; while for circularly polarized incident light, the out-coupling polarization can be further controlled by the orientation of the nano-apertures. This capability also allowed us to create arbitrary vector optical fields, and as an example we generated a radially polarized beam from the circularly polarized incident light. More specifically, we demonstrate a new strategy towards the development of electromagnetic and optical functional devices, where the polarization and phase distributions can be simultaneously manipulated. The demonstration is in the near-infrared wavelength range, which indicates that the approach can be easily translated to mid-infrared, terahertz, and microwave frequency regimes, where the metasurface fabrication and structure alignment should be much easier in addition to lower metal losses. Bringing the new degrees of freedom in designing optical devices to manipulate transmitted light, the plasmonic metasurfaces are expected to impact a wide range of integrated flat optics and photonic applications, ranging from spatial light modulators in holograms[28] to experimental realization of computational metamaterials.[29]

4. Experimental Section

Sample Fabrication: Sputtering deposition, electron-beam lithography, and reactive-ion etching were used to fabricate the metallic structures. The samples shown in Figure 3 for the anomalous refraction and in Figure 4 for the generation of the radially polarized beam were fabricated using the following steps. Au was deposited onto the bare glass substrate to a thickness of 70 nm using a radio-frequency magnetic sputtering system, and a 200-nm-thick PMMA resist was subsequently spin-coated onto the sample; the sample was then subjected to bakeout at 180 °C on a hotplate for 2 min. The pattern was exposed using an electron-beam lithography system (Raith150) at 10 keV. After exposure, the sample was developed in MIBK:IPA (1:3) for 40 s and IPA for 30 s and then blown dry using pure nitrogen. The pattern was transferred onto the Au layer by a reactive-ion etching system using Ar gas. After the PMMA resist was removed with acetone, a 70-nm-thick SiO_2 layer and a 70-nm-thick Au layer were deposited onto the sample using plasma enhanced chemical vapor deposition (PECVD) and a radio-frequency magnetic sputtering system, respectively. The pattern on the second Au layer was prepared by repeating the exposure, etching, and resist-removal processes. Finally, a 70-nm-thick SiO_2 layer was deposited on top of the sample using PECVD.

Measurement Setup for Anomalous Refraction: A mode-locked Ti:sapphire amplified laser provided near-infrared femtosecond laser pulses with a central wavelength of 800 nm, a pulse duration of ~120 fs, and a repetition rate of 1 kHz. The wavelength of light from the laser was tuned over a wide range using an automated optical parametric amplifier (OPAS Prime). A polarizer and a quarter-wave plate (QWP) were combined to generate the incident circularly polarized light, which was focused on the sample with a 20×/0.40 NIR microscope objective. The transmission through the sample was collected using a lens. For the refractive angle detection, we used two concentric rotary systems to achieve independent rotation of the sample orientation and the detector angle. The resolution of the rotation angle was 0.02°. The lens, analyzer, and power meter in the rotary system were used to measure the intensity of light. The analyzer was inserted into the optical path to analyze the polarization status of the transmission light. The other rotary stage was used to adjust the orientation of the sample for oblique incident while the position of the sample was maintained at the center of the stage. This setup allowed us to verify the anomalous refraction phenomenon

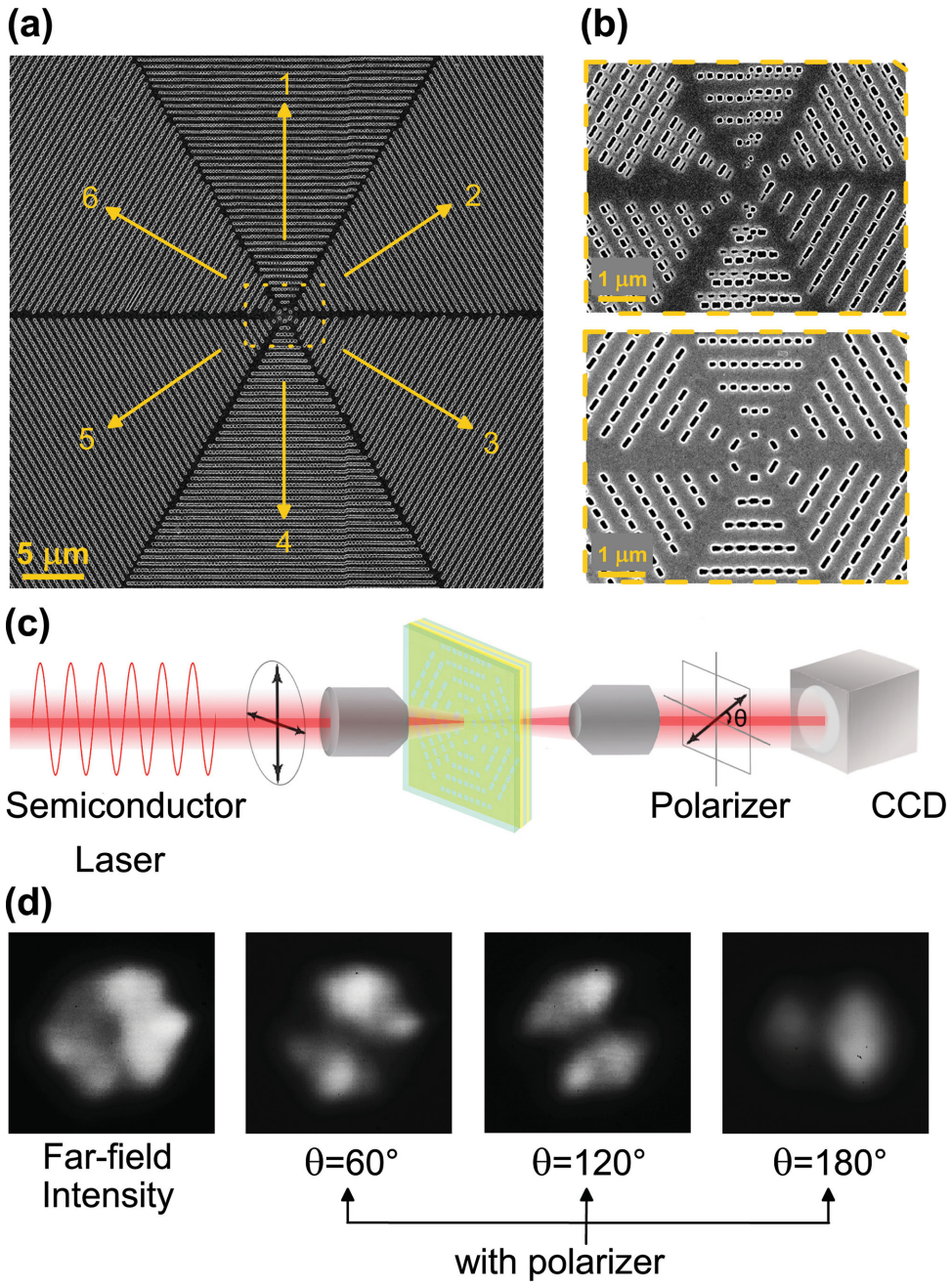

Figure 5. a) SEM image of the plasmonic metasurface to generate a radially polarized beam. Each region of the plasmonic metasurface is filled with one type of nano-aperture pairs marked by the number consistent with that indicated in the most left column in Figure 2b. The yellow arrows represent the designed distribution of the polarization direction. b) Close-up view of the center part of (a) for the upper and bottom layers. c) Schematic of the experimental setup for generating and detecting the radially polarized beam. d) Measured far-field intensity profiles representing a radially polarized beam, without and with a polarizer, where the polarizer was oriented at various angles in front of the CCD camera.

generated by the sample. All the optical elements, including the microscope objective, lens, QWP, polarizer, and detector, were operated in the broadband range.

Supporting Information

Supporting Information is available from the Wiley Online Library or from the author.

Acknowledgements

This work was supported by the National Basic Research Program (973 Program) of China (2012CB921900 and 2009CB930502), the Chinese National Key Basic Research Special Fund (2011CB922003), the Natural Science Foundation of China (61378006, 11304163, 11174362, 91023041, 91323304 and 61390503), the Program for New Century Excellent Talents in University (NCET-13–0294), the Knowledge Innovation Project of CAS (Grand No. KJCX2-EW-W02), the Natural Science Foundation of Tianjin (13JCQNJC01900), and the 111 project (B07013). H.T.C. acknowledges

the partial support from the LANL LDRD program and the Center for Integrated Nanotechnologies.

Received: October 20, 2014
Revised: November 7, 2014
Published online: December 2, 2014

[1] D. G. Grier, *Nature* **2003**, *424*, 810.
[2] M. Liu, T. Zentgraf, Y. Liu, G. Bartal, X. Zhang, *Nat. Nanotechnol.* **2010**, *5*, 570.
[3] N. M. Litchinitser, *Science* **2012**, *337*, 1054.
[4] M. Born, E. Wolf, *Principles of Optics*, Cambridge University Press, Cambridge, UK **1999**.
[5] X. Wang, J. Chen, Y. Li, J. Ding, C. Guo, H. Wang, *Phy. Rev. Lett.* **2010**, *105*, 3966.
[6] H. Chen, J. Hao, B. Zhang, J. Xu, J. Ding, H. Wang, *Opt. Lett.* **2011**, *36*, 3179.
[7] W. Cai, V. Shalaev, *Optical Metamaterials*, Springer Press, New York, USA **2010**.
[8] W. L. Barnes, W. A. Murray, J. Dintinger, E. Devaux, T. W. Ebbesen, *Phys. Rev. Lett.* **2004**, *92*, 107401.
[9] J. A. Schuller, E. S. Barnard, W. Cai, Y. C. Jun, J. S. White, M. L. Brongersma, *Nat. Mater.* **2010**, *9*, 193.
[10] N. Yu, P. Genevet, M. A. Kats, F. Aieta, J.-P. Tetienne, F. Capasso, Z. Gaburro, *Science* **2011**, *334*, 333.
[11] N. K. Grady, J. E. Heyes, D. R. Chowdhury, Y. Zeng, M. T. Reiten, A. K. Azad, A. J. Taylor, D. A. Dalvit, H. T. Chen, *Science* **2013**, *340*, 1304.
[12] N. Yu, F. Capasso, *Nat. Mater.* **2014**, *13*, 139.
[13] S. Sun, K. Y. Yang, C. M. Wang, T. K. Juan, W. T. Chen, C. Y. Liao, Q. He, S. Xiao, W. T. Kung, G. Y. Guo, L. Zhou, D. P. Tsai, *Nano Lett.* **2012**, *12*, 6223.
[14] X. Zhang, Z. Tian, W. Yue, J. Gu, S. Zhang, J. Han, W. Zhang, *Adv. Mater.* **2013**, *25*, 4566.
[15] L. Huang, X. Chen, H. Muhlenbernd, G. Li, B. Bai, Q. Tan, G. Jin, T. Zentgraf, S. Zhang, *Nano Lett.* **2012**, *12*, 5750.
[16] X. Ni, N. K. Emani, A. V. Kildishev, A. Boltasseva, V. M. Shalaev, *Science* **2012**, *335*, 427.
[17] N. Yu, F. Aieta, P. Genevet, M. A. Kats, Z. Gaburro, F. Capasso, *Nano Lett.* **2012**, *12*, 6328.
[18] A. Pors, M. G. Nielsen, R. L. Eriksen, S. I. Bozhevolnyi, *Nano Lett.* **2013**, *13*, 829.
[19] X. Chen, L. Huang, H. Muhlenbernd, G. Li, B. Bai, Q. Tan, G. Jin, C. W. Qiu, S. Zhang, T. Zentgraf, *Nat. Commun.* **2012**, *3*, 1198.
[20] F. Aieta, P. Genevet, M. A. Kats, N. Yu, R. Blanchard, Z. Gaburro, F. Capasso, *Nano Lett.* **2012**, *12*, 4932.
[21] A. V. Kildishev, A. Boltasseva, V. M. Shalaev, *Science* **2013**, *339*, 1232009.
[22] P. Neutens, V. P. Dorpe, I. D. Vlaminck, L. Lagae, G. Borghs, *Nat. Photonics* **2009**, *3*, 283.
[23] F. Miyamaru, M. Takeda, *Phy. Rev. B* **2009**, *79*, 153405.
[24] S. Pancharatnam, *Proc. Ind. Acad. Sci. A* **1956**, *44*, 247.
[25] M. V. Berry, *Proc. R. Soc. London A* **1984**, *392*, 45.
[26] P. Genevet, N. Yu, F. Aieta, J. Lin, M. A. Kats, R. Blanchard, M. O. Scully, Z. Gaburro, F. Capasso, *Appl. Phys. Lett.* **2012**, *100*, 013101.
[27] M. Kang, J. Chen, X. L. Wang, H. T. Wang, *J. Opt. Soc. Am. B* **2012**, *29*, 572.
[28] L. Huang, X. Chen, H. Muhlenbernd, H. Zhang, S. Chen, B. Bai, Q. Tan, G. Jin, K. W. Cheah, C. W. Qiu, J. Li, T. Zentgraf, S. Zhang, *Nat. Commun.* **2013**, *4*, 2808.
[29] A. Silva, F. Monticone, G. Castaldi, V. Galdi, A. Alu, N. Engheta, *Science* **2014**, *343*, 160.